 doi:10.20944/preprints202109.0222.v1

Article

Finite Element Analysis-Aided Optimization of Rectangular Coil Assemblies Applied in Electric Vehicle Inductive Chargers

Guodong Zhu [1] and Dawei Gao [2,*]

[1] State Key Laboratory of Automotive Safety and Energy, School of Vehicle and Mobility, Tsinghua University, Beijing, China; jack.zg68@live.com
[2] State Key Laboratory of Automotive Safety and Energy, School of Vehicle and Mobility, Tsinghua University, Beijing, China; dwgao@mail.tsinghua.edu.cn
* Correspondence: dwgao@mail.tsinghua.edu.cn;

Abstract: Energy efficiency and leakage magnetic field (LMF) are two important issues in electric vehicle inductive chargers. In this work, the maximum achievable coil efficiency and the corresponding LMF strength are formulated as functions of hardware parameters, and figure of merits (FOM) are proposed for assessing the efficiency and LMF performance of the coil assembly pair. The impacts of the coil assemblies' geometric parameters on both FOMs are examined with the aid of finite element analysis (FEA), and measures to improve the FOMs are extracted from FEA results. A coil assembly pair is manually optimized within given dimensional limits. Compared with the initial design, the optimized one achieves higher efficiency and lower LMF strength while consuming less copper. The performance improvement is verified by FEA results and experimental data measured on an 85 kHz electric vehicle inductive charger prototype. The key measures for coil assembly optimization are summarized.

Keywords: efficiency; electric vehicle; finite element analysis; inductive charger; optimization

1. Introduction

Efficiency improvement [1] and leakage magnetic field (LMF) suppression [2] are two important issues in inductive power transfer (IPT) systems, e.g., electric vehicle inductive chargers. The fundamental principle of IPT is to utilize the conversion between electrical energy and magnetic energy as a means of transmitting power over an air gap. Such a conversion is realized via a pair of coil assemblies, one on the transmitter (TX) side and the other on the receiver (RX) side, hence the design of the coil assemblies greatly influences the system performance.

The optimization of coil assemblies has been discussed in numerous references. Some previous works endeavored to maximize the coupling coefficient [3]. Some tried to strike a balance among multiple objectives [4-6]. For most IPT systems, the latter, i.e., multi-objective optimization of the coil assemblies, is of more practical value as a practical IPT system is usually subject to various constraints. Both analytical methods and numerical methods, e.g., finite element analysis (FEA) [3-4] and the finite-difference time-domain method (FDTD) [7-8], are useful tools for performance evaluation. The former is based on simplifications and usually restricted to certain types of systems [5]. By contrast, the latter is universally applicable and highly accurate provided that precise parameters are assigned to the model. A common approach is to combine numerical methods with modern optimization methods, e.g., generic algorithm, to obtain the optimal design in a systematic and efficient manner [3-4]. In this work, FEA (based on the Ansys Maxwell software) is employed to yield quantitative results. Qualitative rules regarding the impact of geometric parameters are extracted, based on which a coil assembly pair is manually optimized to improve the efficiency and LMF performance.

The dominant factors of energy efficiency are mutual inductance and coil ESRs (equivalent series resistance). In a typical electric vehicle inductive charger, a coil

Preprints (www.preprints.org) | NOT PEER-REVIEWED | Posted: 13 September 2021 doi:10.20944/preprints202109.0222.v1

assembly contains three parts: an aluminum shielding plate, a ferrite core and a copper winding. Coil ESR is the combined effect of all three loss terms. The eddy loss in the aluminum plate is related to the ambient magnetic flux density. According to the Steinmetz equation, which is commonly adopted for characterizing magnetic core loss under sinusoidal magnetic field excitations, core loss is approximately a power function of magnetic flux density. Copper loss is influenced by the DC resistance, the skin effect, the proximity effect and other stray factors. When the strand diameter of the Litz wire is below the skin depth, skin effect has a small impact. Proximity effect is related to the magnetic flux density that the copper winding is exposed to [9-10]. Under a given excitation current amplitude, all loss terms are affected by the geometric parameters of the coil assembly. Meanwhile, the output power is proportional to the mutual inductance. Therefore, the maximum achievable energy conversion efficiency of the coil assemblies (designated as η_c and abbreviated as "coil efficiency" in the remaining sections) is influenced by not only coil ESRs but also mutual inductance, and the difficulty in maximizing η_c lies in the fact that both are affected by the geometric parameters in complex ways. To objectively assess the efficiency performance of a coil assembly design, figure of merits (FOMs) that reflect the combined influence of all relevant factors are a useful criterion [11]. Obviously, the η_c-FOM is determined by the geometric parameters of the coil assemblies. Measures to improve η_c via coil assembly optimization have been extensively discussed in previous publications [4, 6, 11].

As for LMF suppression, the measures can be divided into two categories: active suppression [2] and passive shielding [12]. In active suppression schemes, extra coils are usually deployed to generate a magnetic field component that partially counteracts the field generated by the TX and RX coils, thus reducing the overall field strength to an acceptable level. Due to the extra hardware and software cost, such methods are more suitable for high-power applications where passive shielding alone is insufficient. By contrast, passive shielding techniques rely on the design of the coil assembly to reduce the leakage magnetic field strength and are widely adopted due to its simplicity and effectiveness. LMF suppression techniques generally have a negative impact on η_c, and efforts have been made to strike a balance between η_c and the LMF strength [4, 6, 9].

In this article, passive magnetic shielding alone is adopted. Two FOMs are proposed to assess the efficiency performance and the LMF performance of the coil assembly pair applied in electric vehicle inductive chargers. This work is focused on the ferrite layer structure and the copper winding parameters and aims to reveal the impacts of the geometric parameters on the FOMs via the combination of finite element analysis (FEA) and empirical knowledge. A manual optimization procedure under given geometric constraints is conducted with the purpose of improving η_c while having a small impact on the LMF performance. Based on FEA simulations and experimental results obtained from an 85 kHz electric vehicle inductive charger prototype, the superiority of the optimized design is demonstrated. The result is encouraging: the optimized design achieves significantly higher η_c and lower LMF strength while consuming less copper.

The remainder of this article is divided into the following sections. In section 2, the maximum achievable η_c and the corresponding LMF strength are analyzed, and two FOMs are proposed for assessing the efficiency and LMF performance of a coil assembly pair. In section 3, the overall design of the coil assemblies is introduced and the impact of geometric parameters on the FOMs are derived from FEA results. In section 4, the accuracy of FEA in terms of coil loss calculation is verified. Manual optimization of the coil assembly pair is conducted and the superiority of the manually optimized design is validated by FEA results and experimental results. Section 5 gives some discussions. Section 6 concludes this article.

2. Performance Evaluation of Coil Assemblies

2.1 Efficiency Analysis

A simplified schematic of an IPT system with series compensation on both sides is shown in Figure 1. $\boldsymbol{U_{in}}$ is the inverter output voltage, $\boldsymbol{U_L}$ the voltage across the load

Preprints (www.preprints.org) | NOT PEER-REVIEWED | Posted: 13 September 2021 doi:10.20944/preprints202109.0222.v1

resistance, $\boldsymbol{I_1}$ and $\boldsymbol{I_2}$ the coil currents, C_1 and C_2 the series compensation capacitors, L_1 and L_2 the coil inductances, M the mutual inductance, R_L the equivalent AC load resistance, R_1 and R_2 the coil ESRs. Considering that the focus of this work is coil assembly optimization, the power losses in the other components is neglected. Due to the band-pass property of the compensation networks, only the fundamental voltages and currents are considered. For the sake of simplicity, the coil ESRs are assumed to be zero except in efficiency calculations.

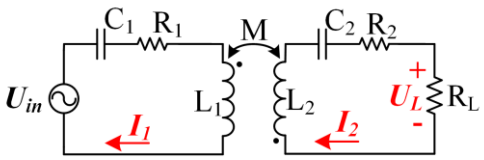

Figure 1. Simplified schematic of series-series-compensated IPT system.

Measures to maximize η_c have been discussed in numerous researches [1]. For the simplified IPT system shown in Figure 1, the output power (P_{out}) is

$$P_{out} = \frac{1}{2}\boldsymbol{I_1} \cdot (j\omega M \boldsymbol{I_2}) \leq \frac{1}{2}\omega M |\boldsymbol{I_1}| \cdot |\boldsymbol{I_2}|. \tag{1}$$

The power loss on coil ESRs is

$$P_{coil} = \frac{1}{2}(|\boldsymbol{I_1}|^2 R_1 + |\boldsymbol{I_2}|^2 R_2) \geq 2P_{out}\frac{\sqrt{R_1 R_2}}{\omega M}. \tag{2}$$

The conditions for minimizing the P_{coil}-to-P_{out} ratio are

$$\angle \boldsymbol{I_1} - \angle \boldsymbol{I_2} = 90^{\circ}, \tag{3-a}$$

$$|\boldsymbol{I_1}|^2 R_1 = |\boldsymbol{I_2}|^2 R_2. \tag{3-b}$$

The first condition is satisfied by maintaining the circuits in full resonance, i.e., $L_1 C_1 = L_2 C_2 = 1/\omega^2$, where ω is the angular operating frequency of the IPT system. In this work, the operating frequency is fixed at 85 kHz. Equation (2) reveals that the lowest achievable P_{coil}-to-P_{out} ratio is a function of $\frac{M^2}{R_1 R_2}$. In this article, this ratio is selected as the FOM for assessing the efficiency performance of the coil assemblies and designated as FOM_{effi}. A larger FOM_{effi} means the maximum achievable η_c is higher. Meanwhile, the optimal AC load resistance that maximizes η_c is

$$R_{L,opt} = \frac{\omega M |\boldsymbol{I_1}|}{|\boldsymbol{I_2}|} = \omega M \sqrt{\frac{R_2}{R_1}}. \tag{4}$$

2.2 *Leakage Magnetic Field Analysis*

LMF is defined as the magnetic field that users might be exposed to under predefined operating conditions, e.g., the magnetic field in the vicinity of an inductively charged electric vehicle. Under the assumption that the flux lines generated by both coil assemblies are overlapped in the LMF region [2], the LMF strength at a selected observation point under conditions (2-a) and (2-b) is simplified as

$$B_{LMF} = \sqrt{k_1^2 |\boldsymbol{I_1}|^2 + k_2^2 |\boldsymbol{I_2}|^2} = \sqrt{\frac{2P_{out}}{\omega M}} \sqrt{k_1^2 \sqrt{\frac{R_2}{R_1}} + k_2^2 \sqrt{\frac{R_1}{R_2}}}, \tag{5}$$

where k_1 or k_2 denotes the magnetic flux density generated by 1 A coil current on the observation point. Therefore, the expression $M \cdot \left(k_1^2 \sqrt{\frac{R_2}{R_1}} + k_2^2 \sqrt{\frac{R_1}{R_2}}\right)^{-1}$ is selected as the

Preprints (www.preprints.org) | NOT PEER-REVIEWED | Posted: 13 September 2021 doi:10.20944/preprints202109.0222.v1

FOM for assessing the LMF performance and designated as FOM_{LMF}. A larger FOM_{LMF} means the LMF strength at the maximum-η_c operating point is lower.

Generally speaking, B_{LMF} increases with coil misalignment, i.e., the highest B_{LMF} is observed when the vehicle-side coil is at the maximum-misalignment position. Still, the FOM_{LMF} calculated based on the k_1 and k_2 data measured at the zero-misalignment position is a useful indicator of the LMF performance. Overall, the LMF strength in the maximum-misalignment case has a positive correlation with that in the zero-misalignment case.

3. Influence of Geometric Parameters

3.1. Overall Design of Coil Assembly Pair

As is shown in Figure 2 (a), a ferrite layer is inserted between the copper winding and the aluminum shielding plate. FEA results reveal that under the same ferrite consumption limit, using an integral ferrite core instead of separate ferrite strips with spaces between them minimizes core loss and eddy loss. In this work, protrusions are added along the outer contour of the ferrite layer to improve mutual inductance and reduce eddy loss. The top view of the coil assembly (excluding the aluminum plate) is given in Figure 2 (b).

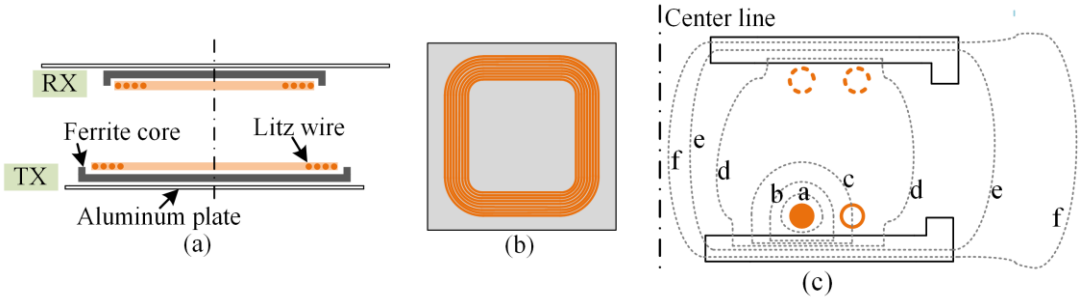

Figure 2. Overall design of the coil assemblies and the magnetic flux paths. (a) Front view. (b) Top view. (c) Magnetic flux paths.

As is illustrated in Figure 2 (c), the magnetic flux lines generated by each turn can be decomposed into six components. Self-inductance is related to the sum of all six components. Mutual inductance is related to the sum of d, e and f. Component f is the source of LMF. Copper loss is mainly affected by components a, b and c.

The geometric parameters influence all six flux components, thereby affecting the system parameters (e.g., k_1, R_1 and M) to different degrees. Take coil ESR as an example. With the strand diameter of the Litz wire being smaller than the skin depth, skin effect is significantly diminished. By contrast, the proximity-effect-induced loss in each strand is caused by the magnetic field strength contributed by all other strands [9-10], including those in the same turn and those that belong to other turns. Therefore, increasing the coil pitch is beneficial for reducing coil ESRs. Meanwhile, when the observation point is located far away from the copper winding, a slight change in coil pitch has a small impact on the winding-to-observation-point distance, hence mutual inductance and LMF strength are less sensitive to the variation of coil pitch. The same conclusion can be derived from the perspective of the magnetic flux components, i.e., coil pitch has a more significant impact on components a, b and c than on d, e and f.

The complexity in coil assembly optimization lies in the fact that the impacts of the geometric parameters on the FOMs are intertwined, hence optimizing one single system parameter, e.g., M, does not necessarily guarantee the best overall performance. For instance, minimizing the coil pitch improves M but lowers FOM_{effi} due to the drastically increased coil ESRs, as will be proved in Figure 4.

Preprints (www.preprints.org) | NOT PEER-REVIEWED | Posted: 13 September 2021 doi:10.20944/preprints202109.0222.v1

3.2 Evaluation of FOMs

3.2.1 Calculation of Coil ESR

FEA is conducted using the Maxwell software contained within the Ansys Electronics Desktop 2020 R2 suite, in which not only the inductances but also the copper loss in Litz wires is obtainable. The main parameter settings are listed in Table 1.

Table 1. Parameter settings in the Maxwell software.

Parameter	Value
Copper conductivity	5.8×10^7 siemens/m
Aluminum conductivity	2.7×10^7 siemens/m
Litz wire diameter	2.45 mm
Litz wire strand diameter	0.1 mm
Litz wire strand number	600
μ_r of ferrite	2200
Coil excitation current	20 A (peak)
Excitation frequency	85 kHz

The ferrite (PC40) core loss density is estimated using the following equation:

$$P_{cv} = 18.7176 f^{1.248} \hat{B}^{2.667}. \quad (6)$$

The units of P_{cv}, f and $\hat{B}$ are W/m^3, Hz and Tesla, respectively. The coefficients are extracted from the loss curves (at 60 degrees Celsius) in the datasheet provided by TDK, Inc. One can infer from (6) that P_{cv} is roughly proportional to $|\boldsymbol{I}_{\boldsymbol{coil}}|^{2.667}$, where $|\boldsymbol{I}_{\boldsymbol{coil}}|$ is the peak value of the coil current. By contrast, copper loss and eddy loss are roughly proportional to $|\boldsymbol{I}_{\boldsymbol{coil}}|^2$. Accordingly, coil ESR is a monotonically increasing function of $|\boldsymbol{I}_{\boldsymbol{coil}}|$.

The influencing factors of coil ESR include copper loss, core loss and eddy loss. FEA results reveal that coil ESR is insensitive to coil misalignment, hence it is reasonable to evaluate coil ESR at the zero-misalignment position only. Geometric symmetry can be employed to greatly reduce the runtime. For instance, a quarter model can be used when the coil assembly is symmetrical with respect to the x- and y-axes.

3.2.2 Evaluation of LMF and Efficiency Performance

The inductances and the LMF strength are directly obtained from the Maxwell software. FEA results show that the LMF strength increases with coil misalignment, hence the LMF performance in the maximum-misalignment case is of the highest practical value. However, as is explained in section 2.2, the LMF strength in the zero-misalignment case is also a good indicator of the LMF performance. Therefore, unless otherwise specified, both the efficiency performance and the LMF performance are evaluated at the zero-misalignment case, so that symmetry can be employed to reduce the model complexity.

To further save the runtime, a coarser mesh is acceptable during LMF strength calculation and inductance calculation. By contrast, a finer mesh is required to improve the precision of ESR calculation.

3.2.3 Impact of Geometric Parameters

The geometric parameters shown in Figure 3 (a) are varied to reveal their impact on the FOMs. The majority of data are obtained in the zero-misalignment case except when the impact of coil misalignment is emphasized, so that a quarter model instead of a full model can be used to save the runtime. The mesh is refined until the results are stable.

Preprints (www.preprints.org) | NOT PEER-REVIEWED | Posted: 13 September 2021 doi:10.20944/preprints202109.0222.v1

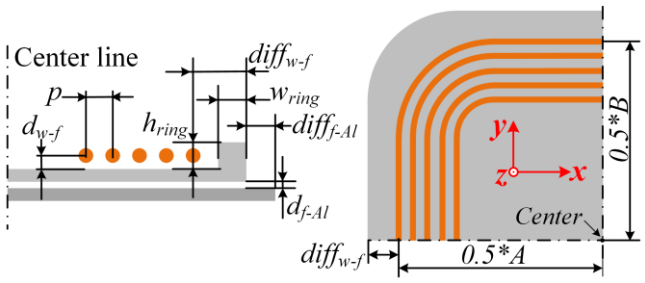

Figure 3. Geometric parameters of the coil assembly (quarter model).

For the sake of simplicity, the rounded corners in the copper winding are omitted in the FEA model. The parameters of the initial design are listed in Table 2. Unless otherwise specified, only one parameter deviates from the initial value during the FEA simulations. The TX- and RX-side coil assemblies have identical geometric parameters, except that the aluminium plate dimensions are different.

Table 2. Initial values of the coil assembly. The unit of all parameters is mm.

Parameter	Value
p	3
A	270
B	270
d_{w-f}	3
d_{f-Al}	2
$diff_{w-f}$	10
$diff_{f-Al}$	5
h_{ring}	0
w_{ring}	5
TX aluminium plate size	300×300×5
RX aluminium plate size	600×600×2
Ferrite core thickness	5
Air gap height	130

Some of the FEA results are presented in Figure 4. Considering that core loss increases faster than copper loss when the excitation current is increased, core loss is increased tenfold in deriving FOM_{effi2} to simulate higher-power operating conditions. When calculating the FOMs, the unit of M, $R_{1/2}$ and $k_{1/2}$ is μH, Ω and μT/A, respectively. The following rules are extracted from the FEA results, some of which are not included in Figure 4. It is virtually impossible to quantify the impacts of geometric parameters on the FOMs, as the impacts are actually dependent upon the initial point. Therefore, the following conclusions are qualitative.

Preprints (www.preprints.org) | NOT PEER-REVIEWED | Posted: 13 September 2021 doi:10.20944/preprints202109.0222.v1

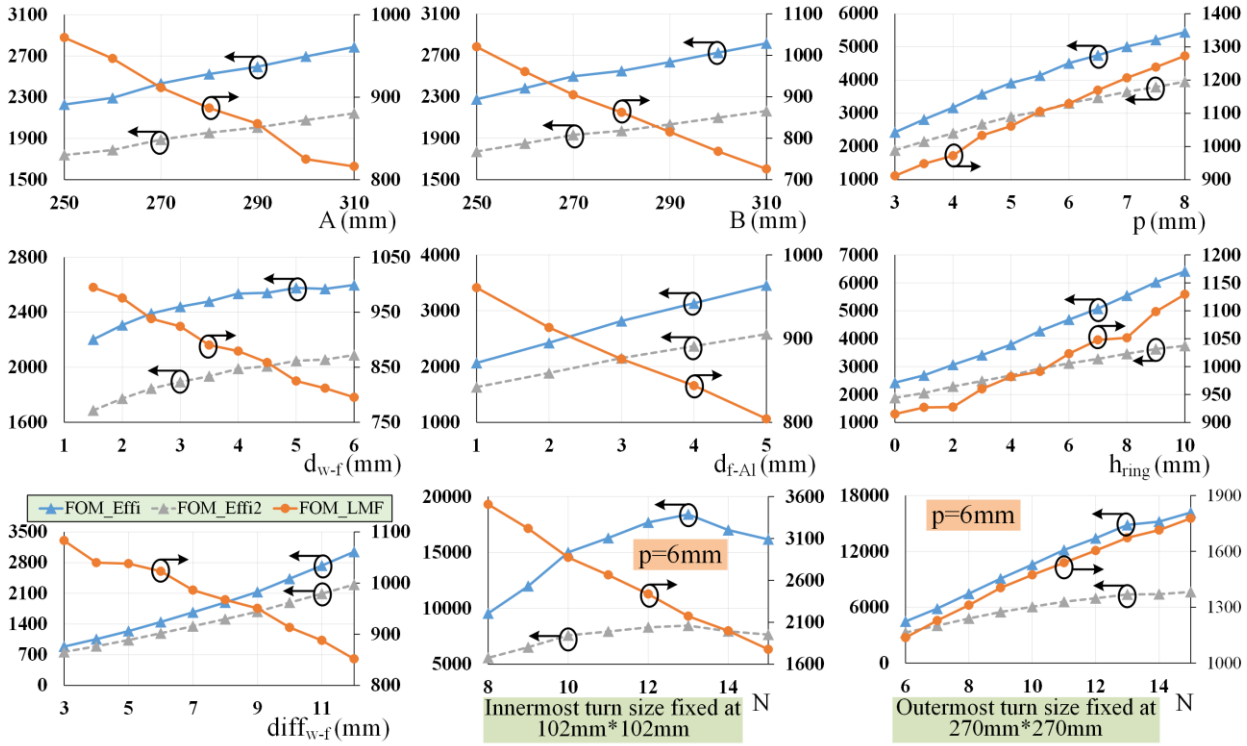

Figure 4. Simulated FOMs. The solid line with triangular dots, dashed line with triangular dots and solid line with circular dots denote FOM_{effi}, FOM_{effi2} and FOM_{LMF}, respectively.

1. With the increase of inter-layer distances (d_{w-f} and d_{f-Al}), FOM_{LMF} is reduced whereas FOM_{effi} is enhanced.
2. Increasing the coil size (A or B) or the ferrite-coil size difference ($diff_{w-f}$) has the same impacts as increasing d_{w-f} does.
3. Adding a ferrite ring, i.e., a protrusion along the outer contour of the ferrite layer, improves both FOMs. By contrast, the impact of w_{ring} is insignificant.
4. The stability of M against coil misalignment can be enhanced via increasing the average turn size of the TX coil. By contrast, increasing the average turn size of the RX coil improves M but has a negligible impact on its stability. In a practical IPT system, higher stability of M means a lighter burden on the power converters, which is favourable. Therefore, the RX coil dimensions should be near the maximum allowable values, whereas the TX coil size is determined by the maximum allowable variation of mutual inductance.
5. Increasing the coil pitch (p) is beneficial for improving both FOMs and the impact is significant. However, for the RX coil, a larger p implies that the maximum allowable turn number is reduced, which can possibly lead to a lower FOM_{effi}. For the TX coil, a larger p means either the turn number or the average turn size is smaller. The possible consequence is either lower FOM_{effi} or lower stability of M, both of which are undesirable. Meanwhile, a lower limit should be imposed on the size of the innermost turn of the RX coil: when the innermost turn is so small that its contribution to mutual inductance is far outweighed by its contribution to coil ESR, increasing the turn number not only consumes more copper wires but also lowers FOM_{effi}.
6. When the outermost turn size is fixed, increasing the turn number before the innermost turn size becomes excessively small is beneficial for improving both FOMs. When the innermost turn size and the ferrite core parameters are fixed, both FOMs are decreased after N exceeds a threshold, which is attributable to eddy loss. By adding a ferrite ring, eddy loss can be effectively suppressed and the maximum allowable outermost turn size is increased.

Preprints (www.preprints.org) | NOT PEER-REVIEWED | Posted: 13 September 2021 doi:10.20944/preprints202109.0222.v1

3.2.4 Constraints and Design Variables

The dimensions of the coil assemblies are subject to various constraints in a practical IPT system. A small profile is preferred for the RX-side coil assembly. By contrast, the TX-side coil should have a relatively large average turn size to improve the stability of M against coil misalignment. Based on Figure 4, the following parameters are fixed to reduce the workload: $h_{ring} = 7mm$, $d_{w-f} = 3.2mm$, $d_{f-Al} = 3mm$. The parameters to be varied during coil assembly optimization are listed below.

- On the TX side: A, B, p, $diff_{w-f}$.
- On the RX side: p, $diff_{w-f}$, N.

The average turn size of the TX coil is determined by N, p and A (B), hence the turn number of the TX coil is subject to the restriction on the stability of M and not a free variable.

4. Optimization of Coil Assemblies

The objectives of coil assembly optimization are to increase both FOMs, particularly FOM_{effi}, enhance the coupling coefficient to reduce the reactive power, and meet the requirement on the stability of M. Due to the large number of geometric parameters and the complex FOM-parameter relations, the optimal design depends on the specific application. The optimal design in this work may be inappropriate for other IPT systems.

4.1 Validation of the Accuracy of FEA

Comparisons are made between FEA results and experimental results to verify the accuracy of the former, as is presented in Figure 5. In the FEA model, the coil current has a constant peak value of 20A. In the experimental measurements, the excitation current provided by the LCR meter (HIOKI IM3536) is 50mArms (at 85kHz). Although both sets of data in Figure 5 do not perfectly match, the overall trend in the FEA results is credible.

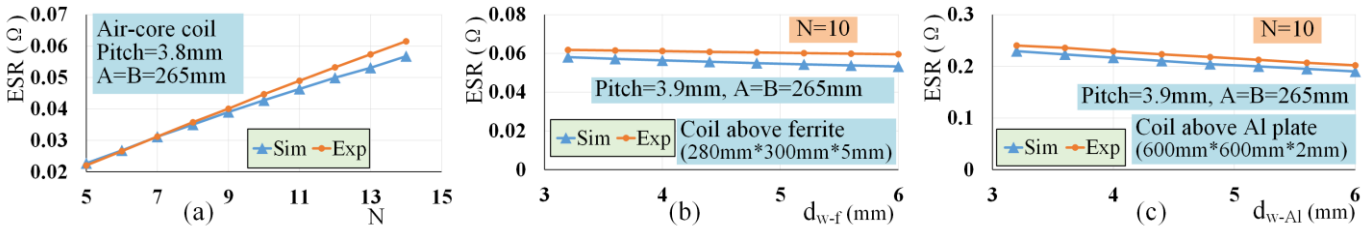

Figure 5. Comparisons between simulated and measured coil ESR. (a) ESR versus N. (b) ESR versus d_{w-f}. (c) ESR versus d_{w-Al} (distance between copper wire and aluminum plate).

4.2 Constraints and Predetermined Parameters

In [13], a manually optimized coil assembly pair with both coil assemblies having identical geometric parameters is compared with the initial design and the performance improvement is proved via FEA results. This work adopts a more practical design in which the TX-side coil assembly has a larger size than the RX-side counterpart. The predetermined parameters are listed in Table 3.

Table 3. Predetermined geometric parameters of the coil assembly pair. The unit of all parameters is mm.

Parameter	Value
Air gap height	160
TX aluminium plate size	560×560×2
RX aluminium plate size	1000×700×2
TX ferrite core size limit	490×490×5
RX ferrite core size limit	360×360×5
Coil misalignment	0 to 100

Preprints (www.preprints.org) | NOT PEER-REVIEWED | Posted: 13 September 2021 doi:10.20944/preprints202109.0222.v1

The test bench adopted in this work is capable of moving along one direction (in the horizontal plane) only, hence coil misalignment is confined to the x axis. The long side of the RX-side aluminum plate is parallel to the x axis.

4.3 Manual Optimization of a Coil Assembly Pair

Based on the conclusions summarized in section 3.2.3, a manual optimization procedure is conducted. The optimized design and the initial design are shown in Figure 6. Because the coils are manually fabricated and the ferrite core is composed of ferrite strips (each measuring 60mm×15mm×5mm), the coil dimensions may appear somewhat odd and the ferrite core dimensions slightly deviate from the limit values. The results obtained from FEA (designated as "simulated") and experimental tests are listed in Table 4. When calculating FOM_{effi}, the unit of M and coil ESR is μH and Ω, respectively. The electric parameters are acquired using an LCR meter (HIOKI IM3536) at an excitation current of 50 mA (rms) with the excitation frequency being 85 kHz.

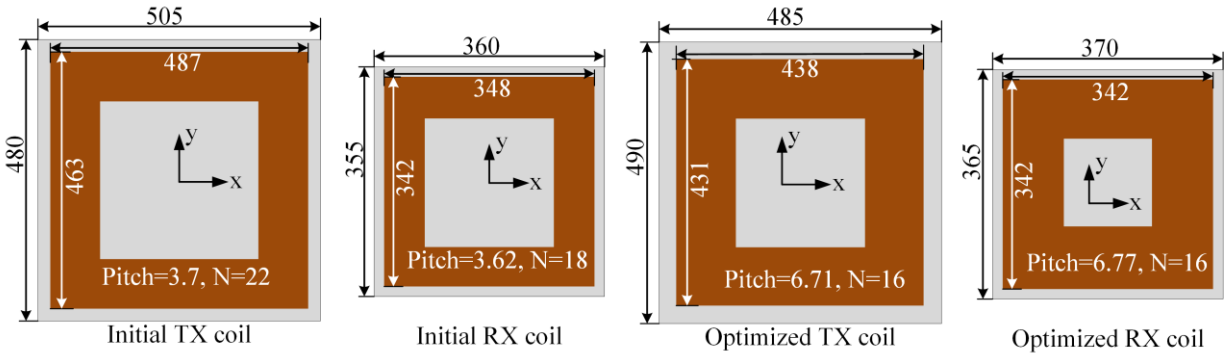

Figure 6. Geometric parameters of the initial and optimized coil assemblies (the aluminum plate is not shown). The coils are made of 600-strand Litz wires.

Table 4. Simulated and measured parameters of the coil assemblies.

Parameter	Initial TX	Initial RX	Optimized TX	Optimized RX
d_{f-Al} (mm)	1.5	1.5	3	3
h_{rng} (mm)	0	0	7	7
Self-inductance (μH)	481.32	223.35	203.25	127.04
DC resistance (mΩ)	141.0	79.8	88.9	67.5
ESR at 85 kHz (mΩ)	616.0	295.1	184.2	139.0
Series capacitance (nF)	7.47	15.64	17.76	27.41
Coupling coefficient	0.107 to 0.138		0.137 to 0.187	
Coupling coefficient (simulated)	0.102 to 0.133		0.129 to 0.181	
Mutual inductance (μH)	35.1 to 45.1		22.0 to 30.1	
FOM_{effi}	6780 to 11193		18924 to 35425	
Litz wire length (m)	55.4		36.8	

The disadvantage of the optimized design is that the mutual inductance drop brought by 100 mm coil misalignment (along the x-axis direction) is 27%, whereas in the initial design the number is 22%. The difference is quite acceptable, though. By contrast, the superiority of the optimized design is obvious. With a 34% reduction in copper wire consumption, both FOM_{effi} and the coupling coefficient are significantly improved. One can easily infer that the VA rating of the series capacitors is greatly reduced.

An electric vehicle inductive charger prototype at an operating frequency of 85 kHz is fabricated based on the parameters in Figure 6. Series compensation is adopted on both sides. The series capacitance values (listed in Table 4) are determined in such a way that the reactance of the coil is almost fully counteracted and the AC impedance seen by the inverter has a small inductive component. A full-bridge passive rectifier composed of SiC

Preprints (www.preprints.org) | NOT PEER-REVIEWED | Posted: 13 September 2021 doi:10.20944/preprints202109.0222.v1

Diodes (Rohm SCS220) is adopted on the RX side. A full-bridge inverter composed of SiC MOSFETs (Cree C3M0075120J) is adopted on the TX side. The power and efficiency data are acquired using a power analyzer (HIOKI PW6001). Photographs of the experimental setup are presented in Figure 7.

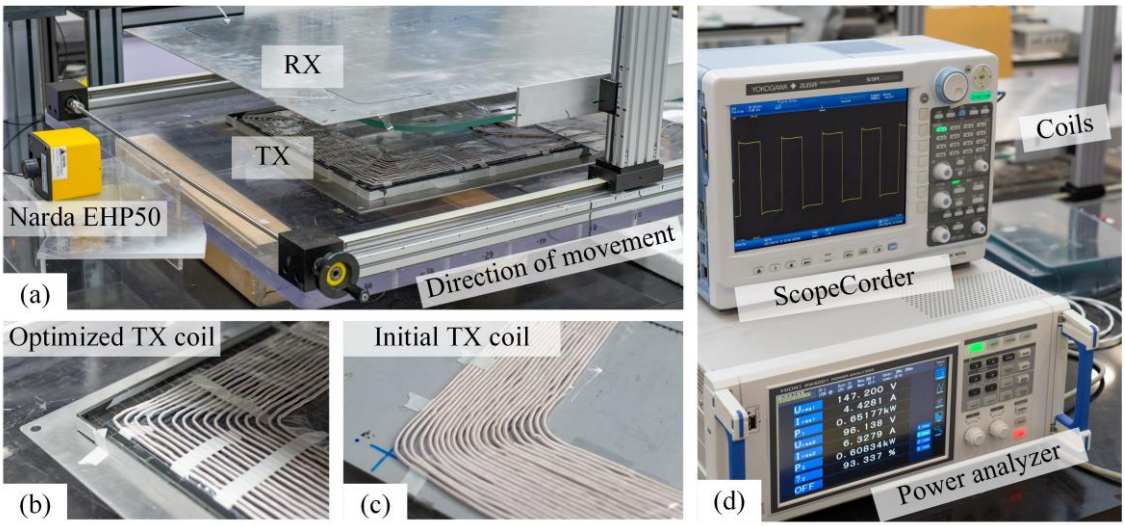

Figure 7. Experimental setup. (a) Coil assembly pair and magnetic field analyser. (b) Optimized TX coil. (c) Initial TX coil. (d) Measurement of power, efficiency and inverter output voltage.

Two DC resistance values are tested: 15 Ω and 20 Ω, which are roughly the optimal load (calculated based on (4)) in the maximum-misalignment and the zero-misalignment cases for the initial design, respectively. The conversion between AC load resistance and DC load resistance is governed by a simple rule: the former is roughly equal to the latter multiplied by $\frac{8}{\pi^2}$. The measured DC-to-DC efficiency at a constant output power of 600W and the DC-link voltage are given in Figure 8. The efficiency improvement brought by the optimization measures is significant. Meanwhile, the stability of mutual inductance, which is reflected in the DC-link voltage curves, is not drastically different in both designs.

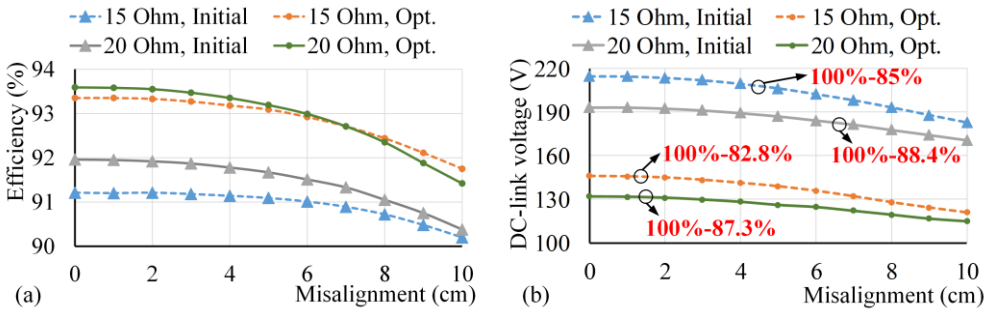

Figure 8. Experimental results. (a) DC-to-DC efficiency. (b) DC-link voltage.

The LMF strength is measured using a magnetic field analyser (Narda EHP50) at a point 70 cm away from the centre of the RX coil. The LMF strength measured in the maximum-misalignment case is listed in Table 5. The LMF performance of the optimized design is slightly better.

Table 5. LMF strength measured in the maximum-misalignment case.

DC load resistance (Ω)	Initial design	Optimized design
15	3.17 μT	2.94 μT
20	3.25 μT	3.11 μT

5 Discussions

Due to unavoidable errors in the geometric and electrical parameters, the FEA results do not strictly match experimentally measured data. Still, the general trend in the FEA results is credible. The DC load resistance adopted in the prototype (15 Ω and 20 Ω) is chosen in such a way that they are equal to the theoretical optimal values for the initial design. For the optimized design, the numbers are approximately 13 Ω and 17 Ω, respectively. The impact of load resistance is clearly displayed in Figure 8. Even with a non-optimal load resistance, the optimized design still outperforms the initial design by a noticeable margin in terms of efficiency and by a small margin in terms of LMF performance.

The key measures for coil assembly optimization are summarized as follows. (1) Coil pitch should be increased to reduce coil ESRs. (2) The average turn size of the TX coil is determined by the required stability of mutual inductance. (3) A ferrite ring should be added and the distance between the outermost turn of the copper winding and the boundary of the ferrite core should be reasonably large to reduce eddy loss.

The findings of this work are applicable to IPT systems other than electric vehicle inductive chargers, as no restrictions specific to electric vehicle charging are imposed during the analysis and optimization procedures.

6. Conclusion

Two FOMs are proposed for evaluating the performance of coil assemblies applied in electric vehicle inductive charging applications. The impacts of the main geometric parameters on both FOMs are examined with the aid of finite element analysis. A manual optimization procedure is conducted based on the qualitative rules extracted from FEA results. In the optimized design, both FOM_{effi} and the coupling coefficient are enhanced. The superior performance of the optimized design is proved via FEA results and experimental tests conducted on an electric vehicle inductive charger prototype. The key measures for coil assembly optimization are summarized.

Author Contributions: Conceptualization, G. Zhu; methodology, G. Zhu; software, G. Zhu; validation, G. Zhu; formal analysis, G. Zhu; investigation, G. Zhu; resources, D. Gao; data curation, G. Zhu; writing—original draft preparation, G. Zhu; writing—review and editing, D. Gao; visualization, G. Zhu; supervision, D. Gao; project administration, D. Gao; funding acquisition, D. Gao. All authors have read and agreed to the published version of the manuscript.

Funding: This research was funded by Beijing Natural Science Foundation, grant number 3212030. The APC was funded by Beijing Natural Science Foundation, grant number 3212030.

Conflicts of Interest: The authors declare no conflict of interest.

References

1. Dai, X.; Li, X.; Li, Y.; Hu, A. P. Maximum Efficiency Tracking for Wireless Power Transfer Systems With Dynamic Coupling Coefficient Estimation. *IEEE Trans. Power Electron.* **2018**, *33*, 5005-5015.
2. Zhu, G.; Gao, D.; Lin, S. Leakage Magnetic Field Suppression Using Dual-Transmitter Topology in EV Wireless Charging. *J. Power Electron*. **2019**, *19*, 625-636.
3. Otomo, Y.; Igarashi, H. A 3-D Topology Optimization of Magnetic Cores for Wireless Power Transfer Device. *IEEE Trans. Magn*. **2019**, *55*, 1-5.
4. Yilmaz, T.; Hasan, N.; Zane, R.; Pantic, Z. Multi-Objective Optimization of Circular Magnetic Couplers for Wireless Power Transfer Applications. *IEEE Trans. Magn*. **2017**, *53*, 1-12.
5. Hariri, A.; Elsayed, A.; Mohammed, O. A. An Integrated Characterization Model and Multiobjective Optimization for the Design of an EV Charger's Circular Wireless Power Transfer Pads. *IEEE Trans. Magn*. **2017**, *53*, 1-4.
6. Bosshard R.; Kolar, J. W. Multi-Objective Optimization of 50 kW/85 kHz IPT System for Public Transport. *IEEE J. Emerg. Sel. Topics Power Electron.* **2016**, *4*, 1370-1382.
7. Kim, M.; Park, S.; Jung, H.-K. Numerical Method for Exposure Assessment of Wireless Power Transmission under Low-Frequency Band. *J. Magn*. **2016**, *21*, 442–449.
8. Park, S. Evaluation of Electromagnetic Exposure During 85 kHz Wireless Power Transfer for Electric Vehicles. *IEEE Trans. Magn*. **2018**, *54*, 1-8.
9. Lu, M.; Ngo, K. D. T. A Fast Method to Optimize Efficiency and Stray Magnetic Field for Inductive-Power-Transfer Coils Using Lumped-Loops Model. *IEEE Trans. Power Electron.* **2018**, *33*, 3065-3075.

10. Wang, X.; Sun, P.; Deng, Q.; Wang, W. Evaluation of AC Resistance in Litz Wire Planar Spiral Coils for Wireless Power Transfer. *J. Power Electron.* **2018**, *18*, 1268–1277.
11. Sampath, J. P. K.; Alphones, A.; Vilathgamuwa, D. M. Coil optimization against misalignment for wireless power transfer. In 2016 IEEE 2nd Annual Southern Power Electronics Conference (SPEC), Auckland, New Zealand, 2016, 1-5.
12. Yashima, Y.; Omori, H.; Morizane, T.; Kimura, N.; Nakaoka, M. Leakage magnetic field reduction from Wireless Power Transfer system embedding new eddy current-based shielding method. In 2015 International Conference on Electrical Drives and Power Electronics (EDPE), Tatranska Lomnica, Slovakia, 2015, 241-245.
13. Zhu, G.; Gao, D. Finite Element Analysis-Aided Performance Improvement of Circular Coil Assemblies Applied in Electric Vehicle Inductive Chargers. In 2021 International Conference on Wireless Power Transfer, 34th International Electric Vehicle Symposium and Exhibition (EVS34), Nanjing, China, 2021.